BEAM DYNAMICS STUDIES FOR THE HIGH-ENERGY STORAGE RING*

A. Lehrach#, B. Lorentz, R. Maier, D. Prasuhn, H. Stockhorst, R. Tölle, D.M. Welsch
Forschungszentrum Jülich, 52425 Jülich, Germany
O. Boine-Frankenheim, R.W. Hasse, S. Sorge
Gesellschaft für Schwerionenforschung, 64291 Darmstadt, Germany
F. Hinterberger
Helmholtz-Institut für Strahlen- und Kernphysik, Universität Bonn, 53115 Bonn, Germany

Abstract

The HESR is planned as an antiproton storage ring in the momentum range from 1.5 to 15 GeV/c. An important feature of this new facility is the combination of phase space cooled beams utilizing electron and stochastic cooling and dense internal targets (e.g. pellet targets).

In this paper different beam dynamics issues like closed orbit correction, performance of cooled beams interacting with internal targets and luminosity considerations are discussed in respect of utilized simulation codes.

INTRODUCTION

The High-Energy Storage Ring (HESR) of the future International Facility for Antiproton and Ion Research (FAIR) at GSI in Darmstadt is planned as an antiproton storage ring in the momentum range from 1.5 to 15 GeV/c [1,2]. The HESR is dedicated to the field of high-energy antiproton physics, to explore the research areas of charmonium spectroscopy, hadronic structure, and quark-gluon dynamics with high-quality beams [3].

Layout and Experimental Requirements

The HESR lattice is designed as a racetrack-shaped storage ring, consisting of two 180° arc sections connected by two long straight sections (see Fig. 1). Special requirements for the lattice are dispersion-free straight sections and small betatron amplitude of about 1 m at the internal interaction point (IP), imaginary transition energy, and optimized ion optical conditions for beam cooling (e.g. matched betatron amplitudes at the pickups and kickers of the stochastic cooling system and in the electron cooler section). Details of the ion optical layout and features of the lattice design are discussed in [4].

Table 1 summarizes the specified injection parameters, experimental requirements and operation modes. Demanding requirements for high intensity and high quality beams are combined in two operation modes: high luminosity (HL) and high resolution (HR), respectively. The high-resolution mode is defined in the momentum range from 1.5 to 9 GeV/c. To reach a momentum resolution down to $\sigma_p / p \sim 10^{-5}$, only 10^{10} circulating particles in the ring are anticipated. The high-luminosity mode requires an order of magnitude higher beam intensity with reduced momentum resolution to reach a luminosity of $2 \cdot 10^{32}$ cm^{-2} s^{-1} in the full momentum range.

Table 1: Beam parameters and operation modes.

Injection Parameters	
Transverse emittance	1 mm·mrad (normalized, rms) for $3.5 \cdot 10^{10}$ particles, scaling with number of accumulated particles: $\varepsilon_{\perp} \sim N^{4/5}$
Relative momentum spread	$1 \cdot 10^{-3}$ (normalized, rms) for $3.5 \cdot 10^{10}$ particles, scaling with number of accumulated particles: $\sigma_p/p \sim N^{2/5}$
Bunch length	Below 200 m
Injection Momentum	3.8 GeV/c
Injection	Kicker injection using multi-harmonic RF cavities
Experimental Requirements	
Ion species	Antiprotons
$\bar{p}$ production rate	$2 \cdot 10^{7}$ /s ($1.2 \cdot 10^{10}$ per 10 min)
Momentum / Kinetic energy range	1.5 to 15 GeV/c / 0.83 to 14.1 GeV
Number of particles	10^{10} to 10^{11}
Target thickness	$4 \cdot 10^{15}$ atoms/cm^2
Transverse emittance	1 to 2 mm·mrad
Betatron amplitude at IP	1 m
Operation Modes	
High resolution (HR)	Luminosity of $2 \cdot 10^{31}$ cm^{-2} s^{-1} for 10^{10} $\bar{p}$ rms momentum spread $\sigma_p / p \sim 10^{-5}$ 1.5 to 9 GeV/c, electron cooling
High luminosity (HL)	Luminosity of $2 \cdot 10^{32}$ cm^{-2} s^{-1} for 10^{11} $\bar{p}$ rms momentum spread $\sigma_p / p \sim 10^{-4}$ 1.5 to 15 GeV/c, stochastic cooling above 3.8 GeV/c

* Work supported by European Community RESEARCH INFRASTRUCTURES ACTION under the FP6 program: DESIGN STUDY (Contract No. 515873 – DIRAC Secondary-Beams), and by INTAS-GSI grants (Ref. No. 03-54-5584).
# a.lehrach@fz-juelich.de

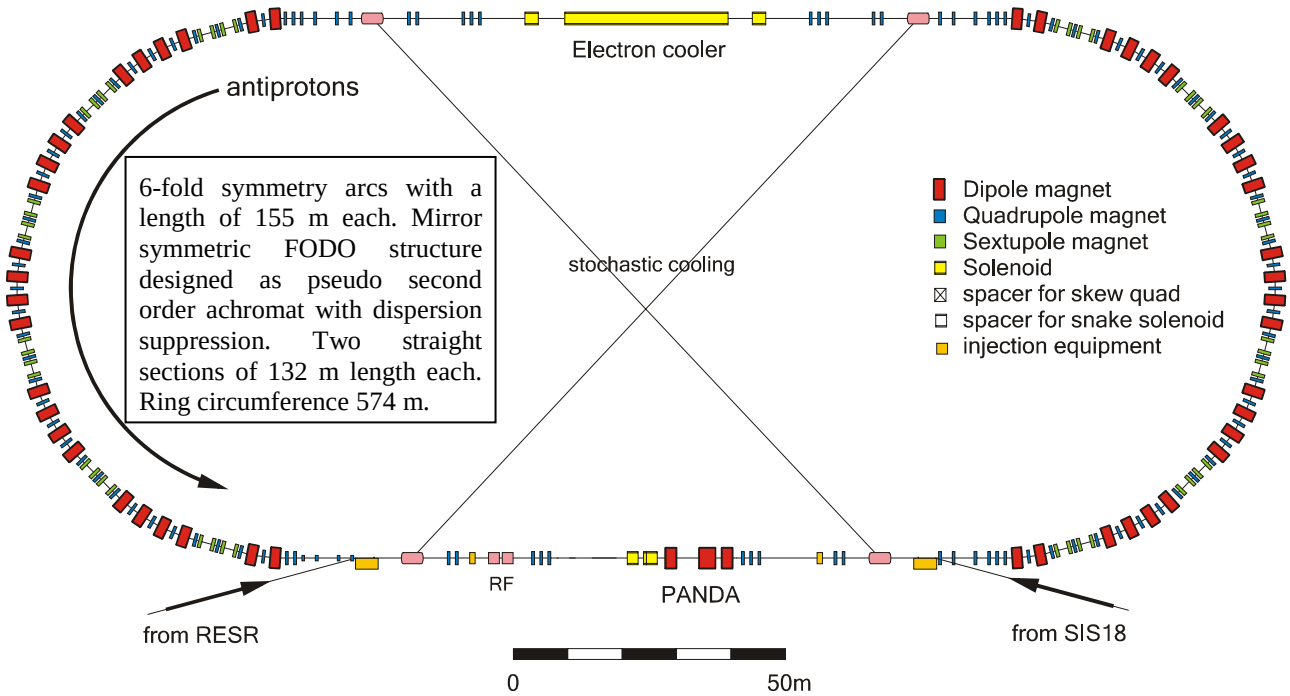

Figure 1: Schematic view of the HESR with 6-fold symmetry lattice. Tentative positions for injection, cooling devices and experimental installations are indicated. One straight section will mainly be occupied by the electron cooler. The other straight section will host the experimental installation with internal frozen H_2 pellet jet target, injection kickers/septa and RF cavities. Two pickup and kicker tanks for stochastic cooling are located close to the ends of the two straight sections, diagonally connected with signal lines.

Beam Dynamics Issues and Simulation Codes

Different beam dynamics calculations have been carried out to ensure beam quality and luminosity in the HESR.

Requirements for RF cavities have been determined utilizing the ORBIT code [5]. RF manipulation of the beam is needed at different stages in the cycle. Two different RF cavity systems are needed for injection, acceleration and storage of antiprotons in the HESR [2].

Further more simulations have been performed with the SIMBAD code [6] to investigate thresholds of the beam's momentum spread due to longitudinal impedances. For this study 10000 macro particles with an overall particle charge of 10^{11} were tracked over 40000 turns [7]. The longitudinal phase space was divided into 128 bins with an initial distribution spread over 360° and $\Delta p/p = 10^{-3}$ to 10^{-5} (rms). As expected from the Keil-Schnell criterion, the momentum spread reaches equilibrium, depending on the total impedance and beam momentum.

The beam intensity and lifetime of the circulating beam can also be limited by the beam of the electron cooler, due to its defocusing effect on the circulating antiproton beam, and coherent instabilities caused by positive residual gas ions trapped in the potential of the electron beam [8,9,10]. The effect of the electron beam on the HESR optics has been studied [11] and some beam disturbing effects have been observed for high electron beam currents exceeding 1A at low beam momentum of HESR.

Dynamic aperture calculations are performed with MAD-X [12] to compensate for non-linear magnetic fields and finally develop a multipole correction concept for the HESR. For the very first study dipole and quadrupole field errors were taken from RHIC: D0 dipole and insertion quadrupole [13]. In the next step we are planning to utilize multipole expansions from calculated field maps of HESR magnets. Furthermore non-linear fields of the electron cooler beam will be included in this simulation. For the description of the interaction between the circulating beam and the electron beam the beam-beam element in the tracking module of MAD-X was extended [14]. A thin-lens approximation was applied to the beam-beam element, describing the interaction between the two beams as transverse beam kicks. For the kicking beam different transverse density distributions can be chosen (e.g. Gaussian or hollow beam). The influence of space charge fields will also be considered.

In this paper we focus on the following beam dynamics items:

- Orbit correction to compensate for positioning errors of magnets and specifications for a steering concept. MAD-X was used and the method of the orbit response matrix applied.
- Investigation of cooled beam equilibria with internal targets utilizing electron and

stochastic cooling were carried out with different simulation codes.

- Analysis of beam losses due to beam-target interaction for luminosity estimations are carried out with analytic formulas.

CLOSED ORBIT CORRECTION

For this investigation [15] the method of orbit response matrix was chosen [16]. Since it is not possible to align all elements perfectly (e.g. magnets and beam position monitors "BPMs"), the trajectories of the circulating particles deviate from the ideal closed orbit. Also field errors of magnets have to be taken into account. The main contribution for the closed orbit deviations are due to angular and spatial positioning error of magnets.

Depending on how one optimizes the position of certain elements, the distribution of the positioning error is changing. If the positioning is done for a maximum value, one expects a uniform distribution. Optimization with highest positioning precision leads to a Gaussian distribution. Positioning errors were applied to dipoles, quadrupoles, correcting dipoles and BPMs. The following error distributions have been utilized to simulate closed orbit deviations (see Table 2). The Gaussian distribution is truncated at 2.5 σ.

Table 2: Width of distribution for positioning errors of magnets and accuracy of BPMs.

Positioning error	Gaussian	Uniform
Angle / mrad	0.55	1.1
Position / mm	0.5	1.0
BPM accuracy	Gaussian	
Scaling	0.1	
Offset / mm	0.1	

A sample of 10 orbits was simulated using the MAD-X code for different seeds generated by a random number generator.

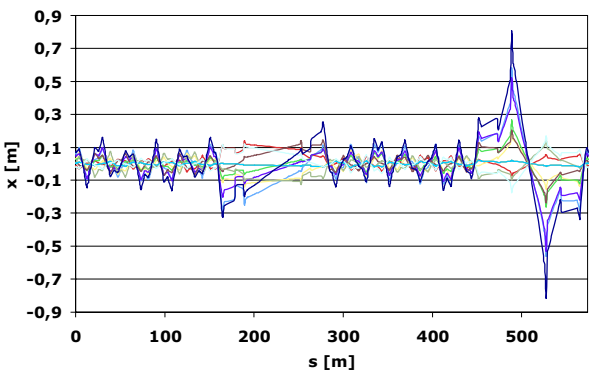

Figure 2: Horizontal closed orbits for different distributed errors vs. longitudinal position in the ring.

In Fig. 2 horizontal closed orbits with Gaussian distributed errors are shown for the horizontal direction. Large closed orbit deviations of more than 800 mm were found in the straight section close to the target (s≈500m), where the betatron amplitude exceeds 500 m. In Fig. 3 the corrected horizontal closed orbits are plotted.

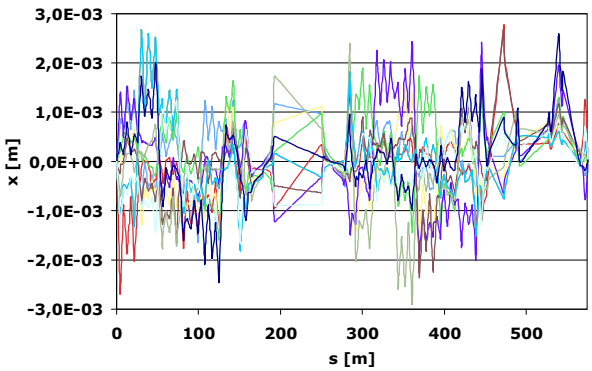

Figure 3: Corrected horizontal closed orbits vs. longitudinal position in the ring.

To prove whether it is realistic to correct the closed orbits to less than 5 mm nearly hundred closed orbits with Gaussian and uniform error distributions have been corrected in both transverse planes. The kick strength of each corrector did not exceed 1 mrad in any case. A total of 48 correcting dipoles in the arcs, and 10 in the straights are placed within the lattice. Due to the betatron functions in the arcs, the correcting dipoles are one-directional, where as the correcting dipoles in the straights correct in both transverse planes. For this correction 72 BPMs in the arcs and 14 in the straights were applied. If one reduces the number of BPMs to 48 in the arcs, the maximum closed orbit correction exceeds 7mm. The method of beam-based-alignment should be applied after beam commissioning to reduce misalignments of the magnets.

Closed-orbit bumps at various positions (e.g. injection point, interaction point, position of beam cooling devices) have been examined to complete the steering concept for HESR. An additional 1 mrad corrector strength is required for orbit bumps, except for the compensation of the electron cooler toroids, where a maximum kick angle of roughly 30 mrad is needed at minimum momentum of the HESR to align the circulating beam [15].

COOLED BEAM EQUILIBRIA WITH INTERNAL TARGETS

Beam equilibrium is of a major concern for the high-resolution mode. Calculations of beam equilibria for beam cooling, intra-beam scattering and beam-target interaction are being performed utilizing different simulation codes like BETACOOL (JINR, Dubna), MOCAC (ITEP, Moscow), and PTARGET (GSI, Darmstadt). Results from different codes for HESR conditions are compared in [17]. Cooled beam equilibria calculations including special features of pellet targets can be carried out with a simulation code based on PTARGET [18].

Electron Cooling

An electron beam with up to 1 A current, accelerated in special accelerator columns to energies in the range of 0.4 to 4.5 MeV is proposed for the HESR. The 24 m long solenoidal field in the cooler section has a field range from 0.2 to 0.5 T with a magnetic field straightness on the order of 10^{-5} [2]. This arrangement allows beam cooling for beam momentum between 1.5 GeV/c and 8.9 GeV/c.

To simulate the dynamics of the core particles, an analytic rms model was applied [19]. The empirical magnetized cooling force formula by V.V Parkhomchuk was used for electron cooling [20], and an analytical description for intra-beam scattering [21]. Beam heating by beam-target interaction is described by transverse and longitudinal emittance growth due to Coulomb scattering and energy straggling, respectively [22,23]. Electron cooler and target parameters for these simulations are electron current of 0.2 A, effective electron velocity of $2 \cdot 10^4$ m/s, and betatron amplitude at electron cooler and target of 100m and 1m, respectively.

Transverse emittance and momentum spread in equilibrium are plotted versus beam energy for the HR mode in Fig. 4.

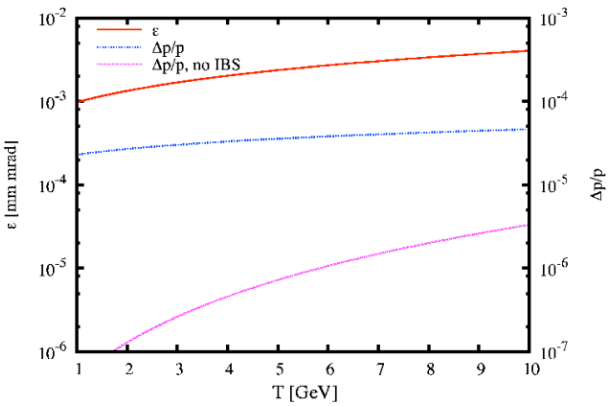

Figure 4: Transverse rms beam emittance (upper curve) and rms momentum spread (two lower curves) in equilibrium vs. kinetic beam energy *T* for the HR mode. Momentum spread equilibria with and without intra-beam scattering are plotted.

Transverse rms beam emittances of about 10^{-3} up to a few times 10^{-2} mm·mrad and rms relative momentum spreads as low as $3 \cdot 10^{-5}$ can be reached in the energy range of the high-resolution mode. The calculations show that the beam equilibria are dominated by intra-beam scattering. Beam heating by the target is at least one order of magnitude weaker. Equilibrium beam emittances do not provide a sufficient beam-target overlap for the HR mode. Proper control of the beam emittance is required by means of external transverse beam heating, beam feedback or artificial deterioration of electron cooling by misaligning the electron beam with respect to the circulating beam.

Stochastic Cooling

The main stochastic cooling parameters were determined for a cooling system utilizing quarter-wave loop pickups and kickers with a band-width of 2 to 4 GHz. Stochastic cooling is presently specified above 3.8 GeV/c [2,24].

Beam equilibria have been simulated based on a Fokker-Planck approach [25]. Longitudinal rms beam equilibrium values are shown in Fig. 5 for both operation modes.

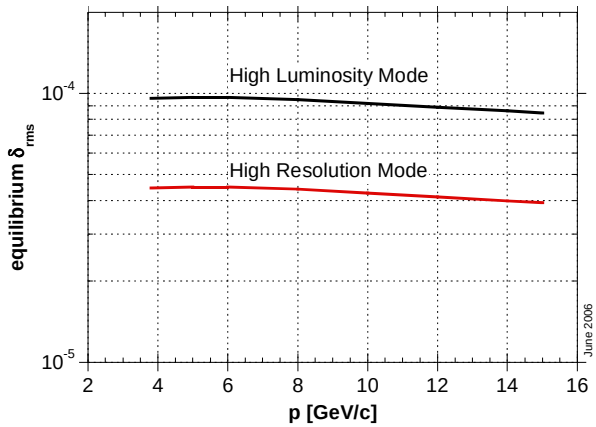

Figure 5: Equilibrium rms momentum spread δ_{rms} vs. beam momentum for the HL and HR mode.

Applying stochastic cooling one can achieve an rms relative momentum spread of 3 to $4 \cdot 10^{-5}$ for the HR mode. In the HL mode rms relative momentum spread slightly below 10^{-4} can be expected. Transverse stochastic cooling can be adjusted independently to ensure sufficient beam-target overlap.

BEAM LOSSES AND LUMINOSITY CONSIDERATIONS

Beam losses are the main restriction for high luminosities, since the antiproton production rate is limited. Three dominating contributions of beam-target interaction have been identified: Hadronic interaction, single Coulomb scattering and energy straggling of the circulating beam in the target. In addition, single intra-beam scattering due to the Touschek effect has also to be considered for beam lifetime estimates. Beam losses due to residual gas scattering can be neglected compared to beam-target interaction, if the vacuum is better than 10^{-9} mbar. A detailed analysis of all beam loss processes can be found in [26,27]

Beam lifetime

The relative beam loss rate for the total cross section σ_{tot} is given by the expression

$$(\tau_{loss}^{-1}) = n_t \sigma_{tot} f_0 , \qquad (1)$$

where (τ_{loss}^{-1}) is the relative beam loss rate, n_t the target thickness and f_0 the reference particle's revolution frequency.

In table 4 the upper limit for beam losses and corresponding lifetimes are listed for a transverse beam emittance of 1 mm·mrad, a longitudinal ring acceptance of $\Delta p/p = \pm 10^{-3}$ and 10^{11} circulating particles in the ring.

Table 4: Upper limit for relative beam loss rate, 1/e beam lifetime t_{pbar}, and maximum luminosity L_{max} for different beam momenta.

(τ_{loss}^{-1}) / s^{-1}			
Heating Process	1.5 GeV/c	9 GeV/c	15 GeV/c
Hadronic Interaction	$1.8\cdot10^{-4}$	$1.2\cdot10^{-4}$	$1.1\cdot10^{-4}$
Single Coulomb	$2.9\cdot10^{-4}$	$6.8\cdot10^{-6}$	$2.4\cdot10^{-6}$
Energy Straggling	$1.3\cdot10^{-4}$	$4.1\cdot10^{-5}$	$2.8\cdot10^{-5}$
Touschek Effect	$4.9\cdot10^{-5}$	$2.3\cdot10^{-7}$	$4.9\cdot10^{-8}$
Total relative loss rate	$6.5\cdot10^{-4}$	$1.7\cdot10^{-4}$	$1.4\cdot10^{-4}$
1/e beam lifetime t_{pbar} /s	~ 1540	~ 6000	~ 7100
L_{max} / 10^{32} cm^{-2}s^{-1}	0.82	3.22	3.93 s

For beam-target interaction, the beam lifetime is independent of the beam intensity, whereas for the Touschek effect it depends on the beam equilibria and beam intensity.

Beam lifetimes are ranging from 1540 s to 7100 s. Beam lifetimes at low momenta strongly depend on the beam cooling scenario and the ring acceptance. Less than half an hour beam lifetime is too small compared to the antiproton production rate.

Luminosity Considerations

The maximum luminosity depends on the antiproton production rate $dN_{pbar}/dt = 2\cdot10^7$ /s and loss rate

$$L_{\max} = \frac{dN_{pbar}/dt}{\sigma_{tot}}, \qquad (2)$$

and is also given in Table 4 for different beam momenta. The maximum luminosity for 1.5 GeV/c is below the specified value for the HL mode.

To calculate the average luminosity, machine cycles and beam preparation times have to be specified. After injection, the beam is pre-cooled to equilibrium (with target off) at 3.8 GeV/c. The beam is then ac-/decelerated to the desired beam momentum. A maximum ramp rate for the superconducting dipole magnets of 25 mT/s is specified. After reaching the final momentum beam steering and focusing in the target and beam cooler region takes place. Total beam preparation time t_{prep} ranges from 120 s for 1.5 GeV/c to 290 s for 15 GeV/c. A typical evolution of the luminosity during a cycle is plotted in Fig. 6 versus time in the cycle.

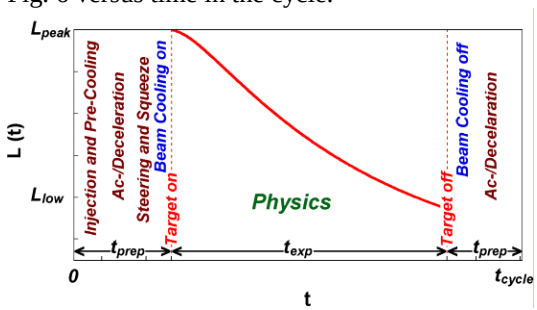

Figure 6: Time dependent luminosity during the cycle *L(t)* versus time in cycle. Different measures for beam preparation are indicated.

In the high-luminosity mode, particles should be re-used in the next cycle. Therefore the used beam is transferred back to the injection momentum and merged with the newly injected beam. A bucket scheme utilizing broad-band cavities is foreseen for beam injection and the refill procedure [2]. During acceleration 1% and during deceleration 5% beam losses are assumed. The average luminosity reads

$$\bar{L} = f_0 N_{i,0} n_t \frac{\tau[1-e^{-\frac{t_{\exp}}{\tau}}]}{t_{\exp}+t_{prep}}. \qquad (3)$$

where τ is the 1/e beam lifetime, t_{exp} the experimental time (beam on target time), and t_{cycle} the total time of the cycle, with $t_{cycle} = t_{exp} + t_{prep}$.

The dependence of the average luminosity on the cycle time is shown for different antiproton production rates in Fig. 7.

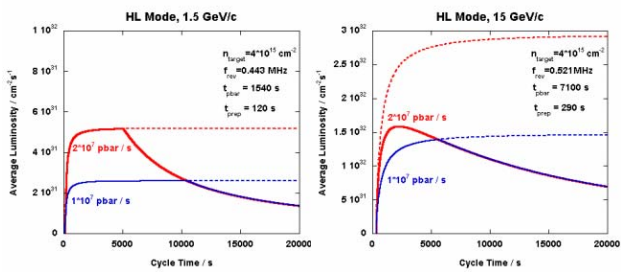

Figure 7: Average luminosity vs. cycle time at 1.5 (left) 15 GeV/c (right). The maximum number of particles is limited to 10^{11} (solid line), and unlimited (dashed lines).

With limited number of antiprotons of 10^{11}, as specified for the high-luminosity mode, average luminosities of up to $1.6\cdot10^{32}$ cm^{-2} s^{-1} can be achieved at 15 GeV/c for cycle times of less than one beam lifetime. If one does not restrict the number of available particles, cycle times should be longer to reach maximum average luminosities close to $3\cdot10^{32}$ cm^{-2} s^{-1}. This is a theoretical upper limit, since the larger momentum spread of the injected beam would lead to higher beam losses during

injection due to the limited longitudinal ring acceptance. For the lowest momentum, more than 10^{11} particles can not be provided in average, due to very short beam lifetimes. As expected, average luminosities are below 10^{32} cm^{-2} s^{-1}.

CONCLUSION AND OUTLOOK

A steering concept for the HESR has been developed, utilizing the method of orbit response matrix. Corrector strengths of less than 1mrad are sufficient to correct the closed orbit deviation below 5mm. Orbit bumps at various position in the ring additionally require 1mrad. Orbit kicks of the circulating beam in the magnet arrangement of the electron cooler have to be corrected.

Different simulation codes have been developed and improved to simulate beam-target interaction of stochastically and electron cooled beams to prove the feasibility of specified operation modes.

Furthermore beam loss mechanisms in the presence of dense internal targets have been identified to get an estimate for average luminosities in the HESR. An optimized beam cooling scenario and larger ring acceptance are required to reach high luminosities close to the theoretical limit.

In a next step a multipole correction scheme is developed. Higher-order field expansions from field calculations of HESR magnets will be utilized together with other non-linear fields like the one generated by the beam of the electron cooler.

REFERENCES

[1] An International Accelerator Facility for Beams of Ions and Antiprotons, Conceptual Design Report, GSI Darmstadt, November 2001, http://www.gsi.de/GSI-Future/cdr/.

[2] FAIR Project (subproject HESR), Technical Baseline Report (March 2006), to be published.

[3] Strong Interaction Studies with Antiprotons, Letter-of-Intent, PANDA collaboration, January 2004, http://www.gsi.de/documents/DOC-2004-Jan-1151.pdf.

[4] Y. Senichev et al., Lattice Design Study for HESR, Proc. of the European Accelerator Conference EPAC, Lucerne, 653 (2004).

[5] J.D. Galambos et al., ORBIT User's Manual, Vers. 1.10, Technical Note SNS-ORNL-AP 0011 (1999); J.D. Galambos, S. Danilov, D. Jeon, J. Holmes, D. Olsen, J. Beebe-Wang, and A.U. Luccio, Proc. of the Particle Accelerator Conference PAC, NY, 3143 (1999).

[6] A.U. Luccio, N. D'Imperio, SIMBAD code, based on ORBIT code, see [5].

[7] A. Lehrach, A.U. Luccio, SIMBAD Studies of the Effect of Impedances on the HESR, 33rd ICFA Advanced Beam Dynamics Workshop, High Intensity & Brightness Hadron Beams ICFA-HB 2004, Bensheim, AIP Conf. Proc.773, 384 (2005).

[8] D.Reistad et al., Measurements of electron cooling and electron heating at CELSIUS, Workshop on Beam Cooling Cool, Montreux, CERN 94-3, 183 (1994).

[9] Yu. Korotaev et al., Intensive Ion Beam in Storage Rings with Electron Cooling, Proc. of the Russian Particle Accelerator Conference RUPAC, Dubna, 13 (2004).

[10] P. Zenkevich, A. Dolinskii and I. Hofmann, Nucl. Inst. Meth. A 532, 454 (2004).

[11] A.U. Luccio, N.D'Imperio, and A. Lehrach, Perturbation of HESR Lattice due to an e-Cool Insertion, 33rd ICFA Advanced Beam Dynamics Workshop, High Intensity & Brightness Hadron Beams ICFA-HB 2004, Bensheim, AIP Conf. Proc. 773, 434 (2005).

[12] MAD-X, Methodical Accelerator Design, Vers. 10, http://mad.web.cern.ch/mad.

[13] M. Anerella et al., Nucl. Inst. Meth. A 499, 280 (2003).

[14] Beam-beam element in the MAD-X tracking module extended by S. Sorge.

[15] D.M. Welsch, Diploma Thesis, Univ. Bonn (September 2006), to be published.

[16] R. Talman, Single particle motion, Frontiers of Particle Beams; Observation, Diagnosis, and Correction, Lecture Notes in Physics, Vol. 343, Springer-Verlag, New York (1888).

[17] A. Dolinskii et al., Simulation Results on Cooling Times and Equilibrium Parameters for Antiproton Beams in the HESR, Proc. of the European Accelerator Conference EPAC, Lucerne, 1969 (2004).

[18] A. Dolinskii et al., Simulation of Pellet Target Effects with the Program PETAG01, this conference.

[19] O. Boine-Frankenheim, R. Hasse, F. Hinterberger, A. Lehrach, P. Zenkevich, Nucl. Inst. and Meth. A 560, 245 (2006).

[20] V.V. Parkhomchuk, Nucl. Inst. Meth. A 441, 9 (2000).

[21] A. H. Sørensen, CERN Accelerator School (edited by S. Turner) CERN 87-10, 135 (1987).

[22] F. Hinterberger, T. Mayer-Kuckuk and D. Prasuhn, Nucl. Instr. Meth. A 275, 239 (1989).

[23] F. Hinterberger, D. Prasuhn, Nucl. Instr. Meth. A 279, 413 (1989).

[24] H. Stockhorst et al., Cooling Scenario for the HESR Complex, Proc. of COOL 2005, Galena, USA (2005).

[25] H. Stockhorst et al., Stochastic Cooling for the HESR at the GSI-FAIR Complex, Proc. of the European Accelerator Conference EPAC, Edinburgh, 231 (2006).

[26] A. Lehrach, O. Boine-Frankenheim, F. Hinterberger, R. Maier, D. Prasuhn, Nucl. Instr. Meth. A 561, 289 (2006).

[27] F. Hinterberger, Beam-Target Interaction and Intra-beam Scattering in the HESR Ring: Emittance, Momentum Resolution and Luminosity, Jül-Report No. 4206 (2006), ISSN 0944-2952.